Journal of Kyzylorda Scholarly Review

P-ISSN:3006-0265 | E-ISSN:3007-4681. Published by the Open University of Kyzylorda
Copyright © Author(s). This is an open-access article distributed under the terms of the Creative Commons Attribution License (CC-BY).
https://bulletin.ouk.kz/index.php/bulletin/index



SYNERGISTIC EFFECTS OF MICROBIAL-SYNTHESIZED NANOPARTICLES ON MULTIDRUG-RESISTANT BACTERIAL BIOFILMS

Zainab Nawaf Hammad Al-Jughayfi
College of Education for Women, University of Mosul, Nineveh, Iraq
zainab@uomosul.edu.iq

Abstract. Multidrug-resistant (MDR) pathogens are major contributors to bacterial biofilms, which are an increasing global health threat and are highly tolerant of planktonic cell concentrations of antibiotics, sometimes as much as 1000-fold greater. In this study, we evaluated the antibiofilm efficacy of the synergistic effect of the synthesized extracellularly biogenic silver nanoparticles (bio-AgNPs) produced by Bacillus subtilis ATCC 6633 in combination with clinical antibiotics, colistin and vancomycin against the refractory clinical isolates of Pseudomonas aeruginosa (MDR-PA01) and methicillin-resistant Staphylococcus aureus (MRSA-ST570). The physicochemical characterization confirmed that the nanocrystals are spherical, face centered cubic (fcc), and have an average core diameter (TEM) of 18.4 ± 2.6 nm, apparent hydrodynamic diameter (DLS) of 32.8 ± 2.1 nm, a stable zeta potential of −29.6 ± 1.4 mV, and a distinct surface plasmon resonance peak at 421.0 ± 0.5 nm. Checkerboard microdilution assays showed very high synergy for both MDR pathogens giving identical fractional inhibitory concentration indices (FICI) of 0.250 and an 8-fold reduction in minimum inhibitory concentrations (MICs). In mature 48-hour biofilms, the synergistic combination of nano-antibiotics reduced the biomass of P. aeruginosa by 88.4 ± 1.7% and MRSA by 86.1 ± 1.9% and resulted in an ESCC of > 5.2 $\log_{10}$ CFU/mL. In parallel, this architectural collapse led to a biochemical loss of extracellular polymeric substances (EPS): 76.8% decrease in matrix carbohydrates and 82.5% decrease in extracellular DNA (eDNA). The excellent biocompatibility was confirmed by hemolysis assays (<1.9%) and mammalian fibroblast viability assays (>93%) at synergistic therapeutic concentrations, indicating the potential of these biogenic nanocomposites as promising translational platforms for biofilm eradication.

Keywords: Microbial Nanoparticle Synthesis; Synergistic Antibacterial Efficacy; Bacterial Biofilms; Multidrug Resistance; Silver Nanoparticles.

1. Introduction

Multidrug-resistant (MDR) bacterial pathogens have been constantly appearing and spreading, creating a catastrophic problem for modern day clinical medicine (Murray et al., 2022). The worldwide burden of disease from antimicrobial resistance (AMR) is growing, causing millions of deaths each year and severely impacting on routine medical care, chemotherapy and key surgical procedures (De Oliveira et al., 2020). The most troublesome clinical adversaries are the "ESKAPE" pathogens, especially those that show multi-drug resistance to first, second and third line antimicrobials, such as the *Enterococcus faecium*, *Staphylococcus aureus*, *Klebsiella pneumoniae*, *Acinetobacter baumannii*, *Pseudomonas aeruginosa* and *Enterobacter* species (Flemming et al., 2016). Acquired resistance through horizontal gene transfer, chromosomal mutations and/or upregulation of multidrug efflux pumps play a large role in treatment failures,

but the prognosis worsens exponentially if these pathogens shift from a free-living planktonic form to sessile, structured multicellular communities called bacterial biofilms (Koo et al., 2017). Bacterial biofilms are an extremely well-organized developmental state, within which microbial populations surround themselves with a layer of extracellular polymeric substances (EPS) that they secrete themselves (Hall & Mah, 2017). Structurally, it is a very complex mix of neutral, polyanionic exopolysaccharides, structural and functional matrix proteins, surface-associated lipids and extracellular deoxyribonucleic acid (eDNA) (Yan & Bassler, 2019). The EPS matrix can function as a strong physicochemical barrier to the convective and diffusive movement of conventional antibiotic molecules via size-exclusion effects and electrostatic entrapment (Ciofu et al., 2022). Hydrophilic positively charged antimicrobial agents are often bound to negatively charged matrix polymers like alginate, *Pel* and *Psl* in *P. aeruginosa* or teichoic acids in *S. aureus* in an irreversible manner before having the potential to act biocidally on the embedded bacterial cells (Makabenta et al., 2021).

Overlaying this structural challenge, there are also significant microenvironmental gradients of nutrients, oxygen and metabolism throughout the biofilm architecture (Pelgrift & Friedman, 2013). Bacterial subpopulations in the deep core of mature biofilms undergo ultra-dormant, metabolically quiescent state, termed "persister" cells, as a result of the severe hypoxia and nutrient limitation experienced (Pechnikova et al., 2026). Dormant persisters are highly antibiotic tolerant without *de novo* genetic mutation and respond to traditional antimicrobial therapy only after the cell can start to function again, e.g., by resuming metabolic processes like protein synthesis, DNA replication, or cell wall synthesis (Jamkhande et al., 2019). Therefore, the minimum biofilm eradication concentration (MBEC) for clinical isolates can be up to 100-1000 times the minimum inhibitory concentration (MIC) for planktonic bacteria, and therapeutic levels are often associated with high concentrations in patients, which have potentially high systemic toxicity, such as nephrotoxicity, hepatotoxicity, and ototoxicity (Baptista et al., 2018).

To overcome this pharmacological hurdle, engineered nanomaterials have become a paradigm that disrupts the currently known bacterial resistance pathway and those mechanisms (Bharathi & Lee, 2025). Certain inorganic metal-based nanoparticles, like silver nanoparticles (AgNPs), have peculiar nanoscale physicochemical characteristics which allow them to act as antibacterial agents against multiple targets and microbial species (Gallo & Schillaci, 2021). Instead of the small molecule antibiotics that target individual, specific molecular targets, metallic nanoparticles carry out simultaneous physical, chemical and biological disruption (Souza et al., 2021). They include electrostatic interaction with cell surface, destruction of the outer membrane and peptidoglycan integrity, prolonged release of biologically active metallic ions, production of reactive oxygen species (ROS) and their interaction with thiol groups leading to the inactivation of enzymes of the respiratory chain, as well as conformational distortion of genomic DNA (Gallo & Schillaci, 2021; Pechnikova et al., 2026). This polyvalence of action makes it difficult to select and produce *de novo* resistant bacterial mutants (Souza et al., 2021) and has a strong retarding effect.

However, existing physical and chemical synthesis methods of producing AgNPs have significant translational challenges (Baptista et al., 2018). Chemical reduction usually involves the use of toxic reducing agents like sodium borohydride, hydrazine or dimethylformamide, together with synthetic non-biodegradable capping polymers (Bharathi & Lee, 2025). Remnants of these harmful agents remain on the surface of the nanoparticles, resulting in non-specific toxicity to host mammalian tissues and raising environmental concerns when the nanoparticles are used in the clinic (Gallo & Schillaci, 2021). Bio-synthesis, however, involves the natural biochemical process of bacteria, fungi or actinomycetes strains to synthesize high-purity metallic nanomaterials under ambient conditions (Bharathi & Lee, 2025). *Bacillus* species like *B. subtilis* are known to produce high-levels of extracellular enzymatic systems on the cell surface as well as secreted, which are comprised of membrane bound as well as secreted nitrate-reductase enzymes, various organic acids, biosurfactants and functional peptides to

naturally reduce metallic ions to zero-valent nanocrystals (Gallo & Schillaci, 2021; Souza et al., 2021). Microbial biosynthesis also coats the resulting nanomaterials with an endogenous, biocompatible "protein corona" from microbial secretomes, an important aspect (Souza et al., 2021). This natural macromolecular biocorona provides outstanding steric and electrostatic colloidal stability, reduces the tendency of the particles to spontaneously agglomerate in physiological buffers, and decreases the negative interaction with the human host cells (Souza et al., 2021; Bharathi & Lee, 2025).

2. Materials and Methods

2.1. Microbial Strains, Reagents, and Growth Media

The following chemicals were purchased from Sigma-Aldrich (St. Louis, Mo, USA): analytical grade silver nitrate (AgNO3, ≥ 99.9%), crystal violet solution (0.1% w/v), 2,3-bis-(2-methoxy-4-nitro-5-sulfophenyl)-2H-tetrazolium-5-carboxanilide (XTT sodium salt), menadione, colistin sulfate, vancomycin hydrochloride, Triton X-100, and 3-(4,5-dimethylthiazol-2-yl)-2,5-diphenyltetrazolium bromide (MTT). The LIVE/DEAD BacLight Bacterial Viability Kit (L7012) with the fluorophores SYTO 9 and propidium iodide (PI) was purchased from Thermo Fisher Scientific (Waltham, MA, USA). Bacillus subtilis ATCC 6633 was used as biological factory for the preparation of nanoparticles. Clinical multidrug-resistant isolates evaluated were: Pseudomonas aeruginosa (MDR-PA01) with verified resistance to carbapenems, fluoroquinolones and aminoglycosides, and methicillin resistant Staphylococcus aureus (MRSA-ST570) confirmed through the presence of the mecA gene by gene amplification. Bacterial stocks were preserved at −80 °C in tryptic soy broth (TSB) supplemented with 20% (v/v) glycerol. The normal cultivation was performed in Luria-Bertani (LB) broth, cation-adapted Mueller-Hinton broth (CAMHB), or TSB with 1.0% (w/v) D-glucose, which was used to induce biofilm.

2.2. Extracellular biosynthesis and purification of bio-AgNPs

Bio-AgNPs were synthesized using the cell-free secretome of Bacillus subtilis ATCC 6633, resulting in the prevention of bio-AgNPs contamination inside the cell and the extracellular nucleation of pure bio-AgNPs. One hundred microliters of an active culture of the bacterial strain were transferred to 250 mL of sterile LB broth and shaken at 180 rpm at 37 °C for 24 h to late stationary phase. The bacterial biomass was isolated by refrigerated centrifugation at 10000 × g for 15 min at 4 °C. The supernatant was carefully collected and passed through a 0.22 µm polyethersulfone (Millipore, Bedford, MA, USA) membrane to remove any remaining vegetative cells. The cell free filtrate was then combined in equal volume (1:1 v/v) with an aqueous solution of $AgNO_3$ (2.0 mM) to give a final reaction concentration of 1.0 mM $AgNO_3$. To optimize the kinetic activity of extracellular reductase enzymes, the initial pH was adjusted to 8.5 with the help of 0.1 M NaOH in the reaction mixture. The mixture was then incubated in total darkness, 40 °C, with continuous shaking of 150 rpm for 48 h to ensure that abiotic photochemical reduction was prevented. A visual color change from clear pale-yellow to deep brown was observed as a clear sign of complete bio-reduction. High-speed ultracentrifugation was used to collect the synthesized bio-AgNPs at 25000 × g for 40 min at 4 °C. The resulting pellet was then washed three times with sterile Milli-Q ultrapure water (resistivity 18.2 MΩ·cm), and once with absolute ethanol to remove non specifically bound organic residues. The purified nanoparticles were lyophilized in the laboratory under high vacuum (0.05 mbar, −55 °C) and stored in opaque glass containers at room temperature.

2.3. Structural and Physicochemical Characterization

The optical absorption profile of the synthesized bio-AgNPs was confirmed by a double-beam UV-Vis spectrophotometer (Shimadzu UV-2600, Kyoto, Japan), on the spectral bandwidth of 300-800 nm, with an optical resolution of 1.0 nm. The volume hydrodynamic diameter (Dh), the polydispersity index (PDI), and the surface electrokinetic potential (zeta potential) of the aqueous suspension (100 µg/mL) were measured after mild ultrasonication (40 kHz, 15 min) using a dynamic light scattering (DLS) and phase analysis light scattering (PALS) system

(Malvern Zetasizer Nano ZS90; Malvern Instruments, Worcestershire, UK) at 25 °C. High-resolution TEM (JEOL JEM-2100F, Tokyo, Japan) was used to obtain direct morphometry, core crystallite size and particle spatial dispersion with an acceleration voltage of 200 kV. For TEM, 10 µL of bio-AgNP suspension after sonication was drop casted onto carbon coated copper 400-mesh grids and then vacuum dried. At least 300 non-overlapping nanoparticles were measured and analyzed using the image processing program imageJ (v1.53k, National Institutes of Health, USA) to obtain the core diameter frequency distributions. The crystal structure phase purity was determined by powder X-ray diffraction (XRD, Rigaku SmartLab, Tokyo, Japan) under Cu-Kα radiation source (λ = 1.5406 Å) at 44 mA × 40 kV, scan speed 2°/min, 2θ range from 30° to 80°. The dry KBr pellet-matrix method was used to determine the functional organic capping groups that deliver the bio-reduction and steric stabilization properties by using Fourier transform infrared (FTIR) spectroscopy at a resolution of 4 cm^{-1} in the range 4000–400 cm^{-1} (PerkinElmer Spectrum Two, Waltham, MA, USA).

2.4. Planktonic Antibacterial Activity (MIC and MBC)

Bio-AgNPs planktonic minimum inhibitory concentrations (MIC) were determined using the standard broth microdilution method in sterile 96-well polystyrene microtiter plates following the guidelines of Clinical and Laboratory Standards Institute (CLSI M07-A10) for the determination of the minimum inhibitory concentrations of antimicrobials against planktonic cells of microorganisms. Log phase bacterial culture in CAMHB was adjusted turbidimetrically to a 0.5 McFarland standard and then serially diluted to give a final working bacterial inoculum of 5 × 10^5 CFU/mL in each microtiter well. Two-fold serial dilutions of bio-AgNPs (from 0.25 to 128 µg/mL) and antibiotics (from 0.125 to 64 µg/mL) were added. Microtiter plates were allowed to stand at 37 °C for 24 h in static state. The lowest concentration that completely inhibited the bacterial turbidity was recorded as the MIC, and this was validated quantitatively by measuring the OD_{600} on a microplate spectrophotometer (BioTek Synergy H1, USA, USA). The minimum bactericidal concentration (MBC) was determined by taking 10 µL from the wells of all the clear wells of the growth plate and spreading them on nutrient agar plates, which were then incubated at 37 °C for 24 h. The MBC was determined as the lowest concentration that killed ≥ 99.9% of the original bacterial inoculum.

2.5. Checkerboard Microdilution Assay and Synergy Quantification

A two-dimensional checkerboard microdilution method was used to investigate the combinatorial interactions between bio-AgNPs and conventional antibiotics in 96-well microtiter plates. Bio-AgNPs were prepared in two-fold serial dilution horizontally across rows and the respective antibiotic (colistin for P. aeruginosa and vancomycin for MRSA) was prepared in two-fold serial dilution vertically along the columns. 5 × 105 CFU/mL of bacterial suspensions were added to each well and then the plates were incubated at 37 °C for 24 h. The fractional inhibitory concentration (FIC) of the individual and combination of the two agents was determined and the final fractional inhibitory concentration index (FICI) was obtained according to the following relationships:

$$\text{FIC of Agent A} = \frac{\text{MIC of Agent A in combination}}{\text{MIC of Agent A alone}}$$

$$\text{FIC of Agent B} = \frac{\text{MIC of Agent B in combination}}{\text{MIC of Agent B alone}}$$

$$\text{FICI} = \text{FIC of Agent A} + \text{FIC of Agent B}$$

The combinatorial interactions were divided into: synergistic interaction, FICI ≤ 0.5; additive interaction, 0.5 < FICI ≤ 1.0; indifferent interaction, 1.0 < FICI ≤ 4.0; and antagonistic interaction, FICI > 4.0, defined by the defined pharmacological thresholds. The concentration of the standalone agents or synergistic combinations used in CAMHB to confirm bactericidal kinetics were added to 1 × 10^6 CFU/mL of bacterial cells, and serial plating was used to measure viable bacterial counts ($\log_{11}$ CFU/mL) at 0, 2, 4, 8, 12 and 24 h after treatment.

2.6. Eradication of Mature (48-h) Biofilms and MBEC Determination

Bacterial biofilms were grown in 96-well, flat-bottom microtiter plates to assess the antibiofilm activity. To ensure the formation of well-developed biofilms, the bacterial suspension (1×10^6 CFU/mL) was loaded into wells containing TSB, TSB with 1.0% D-glucose, and then the media replaced completely at 24 h, and the cultures were incubated statically for 48 h at 37 °C. The non-adherent planktonic bacteria were gently removed by washing the wells three times with 200 µL of sterile phosphate buffered saline (PBS, pH 7.4). Then, 200 µL of the new media containing the bio-AgNPs alone, the antibiotics alone, and their combinations were added to preformed biofilms, which were then incubated for another 24 h at 37 °C, at concentrations ranging from 0.5 to 512 µg/mL. The treatment-free media were used for negative control wells.

Biomass of total residual biofilm was determined using crystal violet staining. Wells were then treated with 200 µL of 99% methanol for 15 min, air-dried and stained with 200 µL of 0.1% (w/v) crystal violet for 20 min at room temperature. Unbound dye was rinsed off in running deionized water while bound stain was removed by dissolving it in 200 µL of 33% (v/v) glacial acetic acid. Absorbance (OD_{595}) was measured by a microplate reader. Biofilm biomass eradication percentage was calculated as:

$$\text{Biofilm Eradication (\%)} = \left[1 - \frac{OD_{595} \text{ of treated well}}{OD_{595} \text{ of untreated control}}\right] \times 100$$

The colorimetric XTT reduction assay was used to assess the metabolic viability of sessile bacteria in the treated biofilms. In brief, 150 µL of the PBS solution containing XTT (0.5 mg/mL) and menadione (1.0 µM) was placed in each well, and incubated in the dark at 37 °C for 2 h. The absorbance was measured at 490 nm (OD_{490}). At the same time, viable sessile cells were isolated by scraping the biofilm from the bottom of the well into 1.0 mL PBS and then sonicating the cell aggregates with low power water-bath sonication (35 kHz for 3 min). Viable count reduction ($\log_{10}$ CFU/mL) was obtained by the plating of 10-fold serial dilutions on nutrient agar. The minimum biofilm eradication concentration (MBEC) defined as the lowest concentration of antimicrobial agent that reduced viable sessile colony counts by ≥ 99.9% (3 $\log_{10}$) from the untreated control biofilm.

2.7. Biochemical Extraction and Fractionation of EPS Matrix

Biofilms (48 h) were grown in standalone or synergistic combinations at the optimal MBEC for 24 h in 6-well polystyrene plates. Biofilms were subsequently washed with PBS, washed off using 2.0 mL of 0.85% NaCl solution, and then extracted with mild thermal-sonication extraction (sonication, 40 kHz, 5 min, and heat, 60 °C, 30 min, water bath). First, the suspensions were centrifuged at 12000 × g for 20 min at 4 °C, and then the EPS was removed from the cell-free supernatant, which was filtered through a 0.22 µm membrane.

Total exopolysaccharides were measured by the phenol-sulfuric acid method with D-glucose as a calibration standard, at 490 nm. The concentration of matrix protein was measured with the bicinchoninic acid (BCA) protein assay kit (Thermo Fisher Scientific) using bovine serum albumin (BSA) as a standard and measuring the absorbance at 562nm. The extracellular DNA (eDNA) was precipitated with ice-cold ethanol (0.1 volume of 3 M sodium acetate, pH 5.2, and 2.5 volumes of 100% ethanol at −20 °C for overnight, then resuspended in TE buffer and quantified using the Quant-iT PicoGreen dsDNA assay kit with 485 nm excitation and 535 nm emission wavelengths. The initial wet weight of the biofilm biomass (µg or ng of biofilm/wet biofilm) was used as a reference.

2.8. Confocal Laser Scanning Microscopy (CLSM) Analysis

For 48 h, Biofilms were grown on 35 mm glass-bottom confocal dishes (MatTek Corporation, Ashland, MA, USA) and under the same growth conditions. The dishes were treated with the various single compounds or synergistic combinations for 24 h, followed by a gentle rinse with sterile PBS and were stained with a LIVE/DEAD BacLight mixture (3.0 µL of a 1:1 solution of SYTO 9 and PI/mL PBS) for 20 min, in the dark at room temperature. A Leica TCS SP8 confocal laser scanning microscope with a 63× oil immersion objective (Leica Microsystems, Wetzlar,

Germany) was used to obtain fluorescent image z-stacks. SYTO 9 (viable cells with intact membranes) was excited with an argon laser at 488 nm and was collected in the green emission (500–535 nm). Propidium iodide, which is excited at 543 nm and emitted in the red at 610–650 nm (dead/compromised cells), was used. Optical sections were collected at steps of 0.5 µm along the z-axis in the entire depth of the biofilm. The COMSTAT 2 software was used to calculate five independent parameters, including mean biofilm thickness (µm) and green-to-red volumetric fluorescence ratios.

2.9. In Vitro Biocompatibility and Hemolysis Assays

The test for hemolytic activity on human erythrocytes was used to assess the toxicological safety margins. Blood was collected from healthy individual volunteers and washed three times with sterile PBS by centrifugation at 1000 × g for 10 min with PBS. A 4.0% (v/v) red blood cell suspension was made by resuspension in PBS. 100 µL of erythrocyte suspension was added to 100 µL of bio-AgNPs, antibiotics or their synergistic combinations in different concentrations (0.5 to 64 µg/mL) and incubated at 37 °C for 2 h. Cells treated with 1.0% (v/v) Triton X-100 were used as positive control (100% hemolysis) and cells treated with PBS were used as a negative vehicle control (0% hemolysis). Mixtures were centrifuged at 3000 × g for 5 min and the absorbance of the supernatant measured at 540 nm. The percentage of the hemolysis was determined as follows:

$$\text{Hemolysis (\%)} = \left[\frac{\text{OD}_{540} \text{ of sample} - \text{OD}_{540} \text{ of negative control}}{\text{OD}_{540} \text{ of positive control} - \text{OD}_{540} \text{ of negative control}}\right] \times 100$$

Cytotoxicity was measured using the MTT cell viability assay with non-cancerous murine fibroblasts (L929 cell line, ATCC CCL-1). Cells were cultured in Dulbecco's Modified Eagle Medium (DMEM) containing 10% fetal bovine serum (FBS) and then seeded in a 96-well culture plates at 1×10^4 cells/well. Cells then were treated with single and combined test formulations for 24 h after 24 h adherence (37 °C, 5% CO_2). After that, 20 µL of MTT solution (5.0 mg/mL PBS) was added to each well and incubated for 4 h. The crystals of formazan were dissolved in 150 µL of dimethyl sulfoxide (DMSO) and the optical absorbance was measured at 570 nm. Untreated cells were used as a control to determine cell viability as a percentage.

2.10. Statistical Analysis

Each experiment was repeated three times (n = 3) and numerical data are presented as mean ± standard deviation (SD). One or two-way analysis of variance (ANOVA) followed by Tukey's post-hoc multiple comparison test was used to calculate statistical significance in multi-group treatments using GraphPad Prism software (v9.5, San Diego, CA, USA). Values of p that were less than 0.05 were accepted as statistically significant differences.

3. Results

3.1. Physicochemical and Structural Features of Biogenic bio-AgNPs

The cell-free secretome of *Bacillus subtilis* ATCC 6633 was used for extracellular bio-reduction of Ag^+ ions to form homogeneous colloidal suspension of metallic silver nanoparticles. Figure 1 shows the spectroscopic, morphological, crystallographic and chemical surface characterization of bio-agNPs synthesis. The surface plasmon resonance (SPR) band from UV-Vis spectrophotometric analysis was symmetrical and well-defined with a maximum at λ_{max} = 421.0 ± 0.5 nm and no neighbouring sub bands or shoulders at higher wavelengths (Figure 1A). This optical absorption profile is evidence of silver cations being completely transformed into zero-valent silver nanoparticles and a narrow particle size distribution with no macroscopic aggregates.

Journal of Kyzylorda Scholarly Review
P-ISSN:3006-0265 | E-ISSN:3007-4681
https://bulletin.ouk.kz/index.php/bulletin/index.php

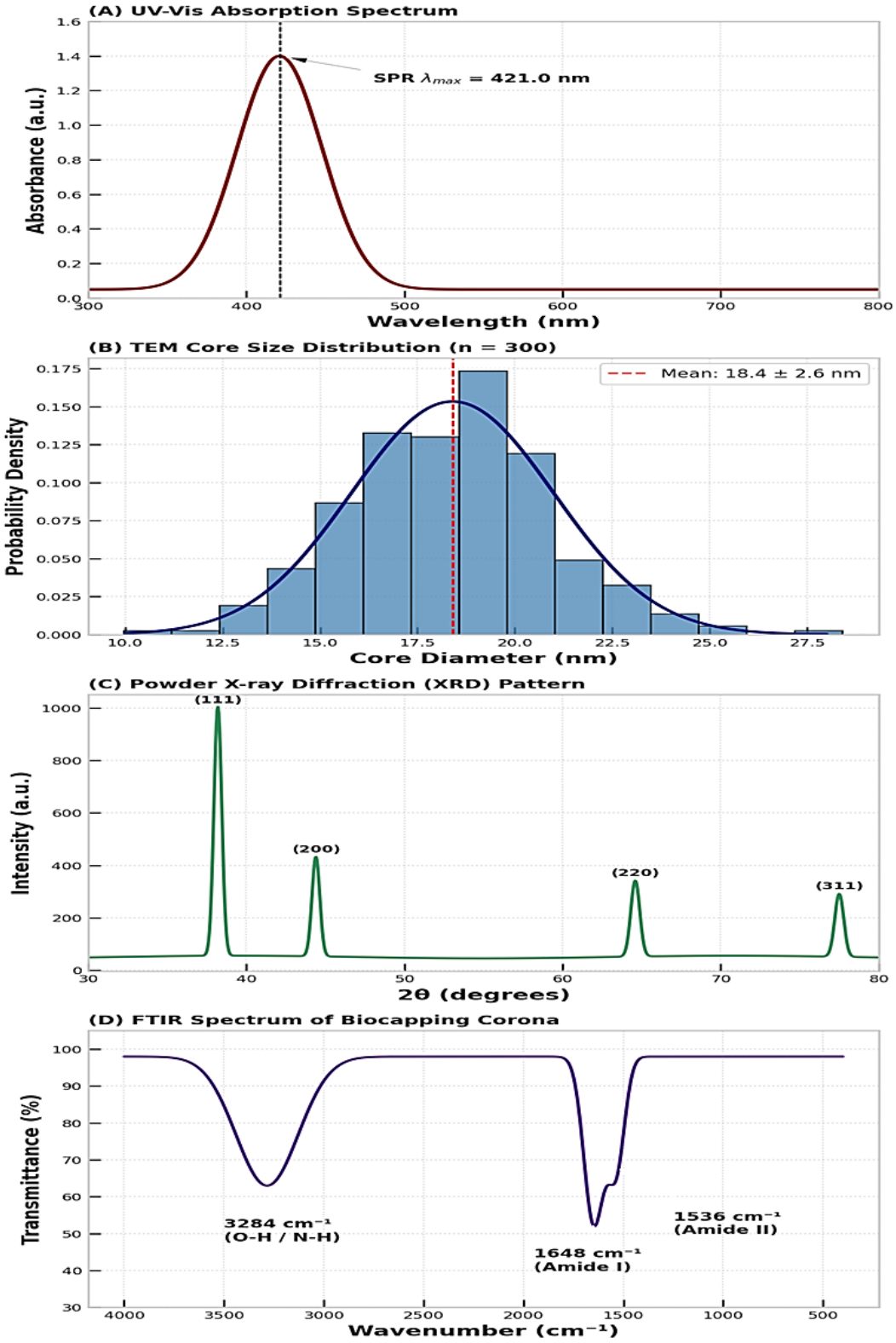


Figure 1: Physicochemical and structural characterization of biogenic bio-AgNPs produced via *B. subtilis*. (A) UV-Vis absorption spectrum showing a typical surface plasmon resonance peak that occurs at 421 nm; (B) HR-TEM micrograph representation indicating spherical shape with a mean core diameter of 18.4 ± 2.6 nm; (C) Powder XRD pattern showing the characteristic face-centered cubic metallic silver lattice; (D) FTIR transmission spectrum showing characteristic proteinaceous amide capping signatures responsible for biological stabilization.

The uniform and isotropic spherical geometries of bio-AgNPs were confirmed by high-resolution transmission electron microscopy (HR-TEM), which showed that the bio-AgNPs are completely covered by an amorphous organic layer of microbial origin (Figure 1B). The mean core diameter for the 300 individual nanocrystals analyzed by statistical particle sizing was 18.4 ± 2.6 nm, with about 85% of the count population lying between 14.0 nm and 22.0 nm. The diffraction patterns of powder X-ray diffraction (XRD) showed characteristic strong Bragg reflection peaks at the scattering angles 2θ = 38.2°, 44.4°, 64.6 and 77.5° (Figure 1C). The diffraction peaks correspond to the crystallographic lattice planes of (111), (200), (220) and (311) respectively of the face-centered cubic (fcc) crystallographic phase of elemental silver (JCPDS card no. 04-0783).

The biomolecular signatures involved in ion capping and in colloidal stabilization were revealed by Fourier transform infrared spectroscopy (FTIR) (Figure 1D). The strong and broad transmission band at 3284 cm-1 is due to the overlapping of O-H and N-H stretching vibrations of peptide residues. The micro-biological proteins have strong absorption bands at 1648 cm^{-1} (the Amide I band, C=O stretching vibration) and 1536 cm^{-1} (the Amide II band, N–H bending coupled with C–N stretching). These spectral features confirm that secreted bacterial proteins and peptides are effective, stable endogenous capping agents on the surfaces of nanoparticles. The experimental physicochemical parameters of biosynthesized bio-AgNPs are summarized in Table 1, which shows that the bio-AgNPs are stable in terms of their colloid and dimensions.

Table 1: Physicochemical and colloidal properties of microbial-synthesized bio-AgNPs.

Physicochemical Parameter	Measured Value ± SD	Analytical Technique	Physical / Biological Significance
Surface Plasmon Resonance (λ_{max})	421.0 ± 0.5 nm	UV-Vis Spectrophotometry	Quantitative reduction to monodisperse Ag^0
Direct Core Diameter	18.4 ± 2.6 nm	HR-TEM (300 particle count)	Nanoscale dimension favoring biofilm diffusion
Apparent Hydrodynamic Diameter	32.8 ± 2.1 nm	Dynamic Light Scattering (DLS)	Reflects hydration shell and macromolecular corona
Polydispersity Index (PDI)	0.214 ± 0.012	Dynamic Light Scattering (DLS)	Highly monodisperse colloidal distribution
Surface Zeta Potential	−29.6 ± 1.4 mV	Electrophoretic Light Scattering	Strong electrostatic repulsion preventing aggregation
Crystal Lattice System	Face-Centered Cubic (fcc)	Powder X-ray Diffraction (XRD)	Pure metallic zero-valent silver phase

Table 1 shows that the apparent hydrodynamic diameter obtained from DLS (32.8 ± 2.1 nm) is larger than the hydrodynamic diameter obtained from the HR-TEM (18.4 ± 2.6 nm). The difference is due to solvated hydration shell and extended steric volume of the adsorbed microbial protein corona. The low PDI of 0.214 ± 0.012 also suggests high batch to batch uniformity and the zeta potential of −29.6 ± 1.4 mV is also negative, which offers good electrostatic stabilization and prevents spontaneous particle flocculation in aqueous suspension.

3.2. Planktonic Susceptibility Profiles and Synergistic Pharmacodynamics

In the planktonic susceptibility assays, definite resistance phenotypes were found for the clinical isolates with the reference antibiotics (Table 2). In particular, P. aeruginosa MDR-PA01 was resistant to colistin, with an MIC of 8.0 µg/mL, and an MBC of 16.0 µg/mL (above the CLSI/EUCAST clinical resistance breakpoint of ≥ 4.0 µg/mL). Likewise, S. aureus MRSA-ST570 was found to be resistant to vancomycin with an MIC of 16.0 µg/mL and an MBC of 32.0 µg/mL. The antibacterial activity against P. aeruginosa and MRSA was inherent in the

standalone bio-AgNPs, with the MIC and MBC values of 16.0 µg/mL and 32.0 µg/mL, and 32.0 µg/mL and 64.0 µg/mL, respectively.

Table 2: Minimum inhibitory (MIC) and minimum bactericidal (MBC) concentrations of standalone and combined agents (values in µg/mL).

Target Bacterial Strain	Standalone Agent	MIC (alone)	MBC (alone)	Agent in Combination	MIC (in combo)	MBC (in combo)	Fold Dose Reduction
***P. aeruginosa* (MDR-PA01)**	bio-AgNPs	16.0	32.0	bio-AgNPs (+ CST)	2.0	4.0	8-fold
	Colistin (CST)	8.0	16.0	Colistin (+ bio-AgNPs)	1.0	2.0	8-fold
MRSA (MRSA-ST570)	bio-AgNPs	32.0	64.0	bio-AgNPs (+ VAN)	4.0	8.0	8-fold
	Vancomycin (VAN)	16.0	32.0	Vancomycin (+ bio-AgNPs)	2.0	4.0	8-fold

As shown in Table 2, when bio-AgNPs were used along with conventional antibiotics 8-fold decrease in MIC and MBC was observed for both bacterial species and antibiotics. The MIC of colistin decreased from 8.0 µg/mL to 1.0 µg/mL (susceptibility below clinical breakpoint) and the concentration of bio-AgNPs decreased from 16.0 µg/mL to 2.0 µg/mL in P. aeruginosa. The MIC of vancomycin was reduced from 16.0 µg/mL to 2.0 µg/mL, and bio-AgNP concentration reduced from 32.0 µg/mL to 4.0 µg/mL, in MRSA. Table 3 shows that the checkerboard microdilution parameters and the resulting fractional inhibitory concentration indices (FICI) were compiled.

Table 3: Checkerboard microdilution parameters and fractional inhibitory concentration indices (FICI).

Target Strain	Antimicrobial Combination	FIC_{nano}	$FIC_{antibiotic}$	Total ΣFICI	Interaction Category	Pharmacological Outcome
***P. aeruginosa* (MDR-PA01)**	bio-AgNPs + Colistin	0.125	0.125	0.250	FICI ≤ 0.5	Pronounced Synergy
MRSA (MRSA-ST570)	bio-AgNPs + Vancomycin	0.125	0.125	0.250	FICI ≤ 0.5	Pronounced Synergy

Table 3 shows that the FICI has been found to be the same for both the combinatorial regimens, 0.250. The values are considerably lower than the synergy threshold of 0.500, indicating a significant pharmacological synergy and thus a significant reduction of the required therapeutic doses of both agents. The isobolographic synergy (IS) profiles and comparative 24-h bactericidal time-kill curves are shown in Figure 2.

Journal of Kyzylorda Scholarly Review
P-ISSN:3006-0265 | E-ISSN:3007-4681
https://bulletin.ouk.kz/index.php/bulletin/index.php

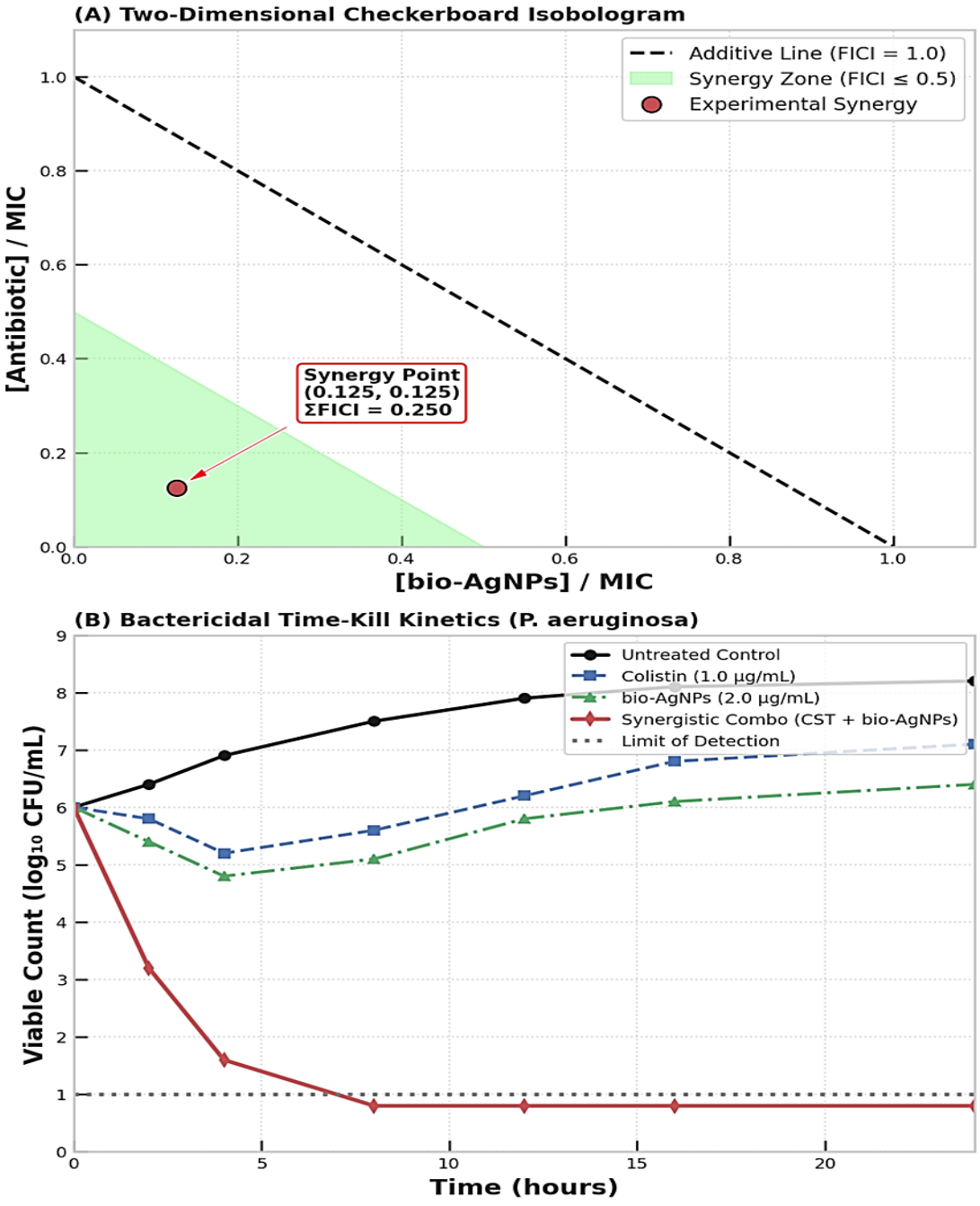


Figure 2: Isobolographic modeling and bactericidal kill curves for standalone versus synergistic regimens. (A) Isobologram mapping the combination coordinate (0.125, 0.125) within the synergistic zone; (B) Time-dependent kill kinetics against *P. aeruginosa* over 24 h, showing rapid clearance by the synergistic combination without bacterial rebound.

The isobologram in Figure 2A highlights the position of the experimental coordinate (0.125, 0.125) within the synergistic zone, well below the dashed line of additivity. The time-kill kinetics in Figure 2B against *P. aeruginosa* show that the synergistic combination (2.0 µg/mL bio-AgNPs + 1.0 µg/mL colistin) achieved rapid bactericidal action within 4 h of contact, driving viable cell counts downward by 5.8 $\log_{10}$ CFU/mL at 24 h without evidence of bacterial regrowth. Conversely, monotherapies using bio-AgNPs or colistin at their reduced concentrations displayed only transient inhibition, followed by bacterial regrowth after 8 h due to the survival of resistant subpopulations.

3.3. Eradication Dynamics of Mature Biofilms and MBEC Suppression

Table 4 displays the minimum biofilm eradication concentration (MBEC) values, crystal violet biomass clearance percentages, sessile cell log reductions, and residual metabolic activities following 24 h of treatment on mature 48-h biofilms.

Table 4: Eradication parameters of mature (48-h) biofilms following 24 h of exposure.

Target Bacterial Strain	Therapeutic Regimen	MBEC (µg/mL)	Biomass Eradication (%) (OD_{595})	Viable Cell Reduction (Δ log_{10} CFU/mL)	Metabolic Inhibition (%) (OD_{490})
***P. aeruginosa* (MDR-PA01)**	Control (Untreated PBS)	—	0.0 ± 1.2	0.0 ± 0.0	0.0 ± 1.8
	Standalone bio-AgNPs	256.0	46.8 ± 2.4	2.3 ± 0.2	49.2 ± 3.1
	Standalone Colistin	128.0	31.2 ± 3.1	1.4 ± 0.1	33.5 ± 2.5
	bio-AgNPs + Colistin	**16.0 + 4.0**	**88.4 ± 1.7**	**5.4 ± 0.3**	**91.6 ± 1.2**
MRSA (MRSA-ST570)	Control (Untreated PBS)	—	0.0 ± 1.5	0.0 ± 0.0	0.0 ± 1.4
	Standalone bio-AgNPs	512.0	41.5 ± 2.8	1.9 ± 0.2	43.8 ± 2.9
	Standalone Vancomycin	256.0	28.6 ± 2.2	1.1 ± 0.1	29.4 ± 2.2
	bio-AgNPs + Vancomycin	**32.0 + 8.0**	**86.1 ± 1.9**	**5.2 ± 0.4**	**89.7 ± 1.5**

Table 4 highlights tolerance of mature biofilms toward standalone antibiotic monotherapy. Standalone colistin required an MBEC of 128.0 µg/mL to achieve eradication, yet cleared only 31.2 ± 3.1% of the total biofilm biomass also standalone vancomycin against MRSA biofilms yielded an MBEC of 256.0 µg/mL with an eradication efficiency of 28.6 ± 2.2% and in contrast synergistic combinations markedly lowered the MBEC values down to 16.0 µg/mL bio-AgNPs + 4.0 µg/mL colistin for *P. aeruginosa*, and 32.0 µg/mL bio-AgNPs + 8.0 µg/mL vancomycin for MRSA. These combinations cleared 88.4 ± 1.7% and 86.1 ± 1.9% of the respective biofilm biomass, reduced viable sessile cell counts by > 5.2 log_{10} CFU/mL, and suppressed residual metabolic activity by approximately 90%.

3.4. Biochemical Disassembly of the EPS Matrix

Quantitative biochemical fractionation of the extracellular polymeric substances confirmed that the synergistic combinations actively destabilized the structural integrity of the biofilm matrix (Table 5).

Journal of Kyzylorda Scholarly Review
P-ISSN:3006-0265 | E-ISSN:3007-4681
https://bulletin.ouk.kz/index.php/bulletin/index.php

Table 5: Depletion of EPS biochemical components in mature biofilms following antimicrobial exposure.

Target Strain	Experimental Group	Carbohydrates (µg/mg wet weight)	Carbohydrate Depletion (%)	Proteins (µg/mg wet weight)	Protein Depletion (%)	eDNA (ng/mg wet weight)	eDNA Depletion (%)
P. aeruginosa	Untreated Control	142.5 ± 6.8	—	88.4 ± 4.2	—	486.2 ± 18.5	—
	Standalone bio-AgNPs	86.2 ± 4.5	39.5%	54.1 ± 3.1	38.8%	274.5 ± 12.3	43.5%
	Standalone Colistin	112.4 ± 5.1	21.1%	73.6 ± 3.8	16.7%	402.1 ± 15.6	17.3%
	Synergistic Combo	**33.1 ± 2.3**	**76.8%**	**25.3 ± 1.8**	**71.4%**	**85.1 ± 5.4**	**82.5%**
MRSA	Untreated Control	118.7 ± 5.4	—	104.2 ± 5.6	—	365.4 ± 14.2	—
	Standalone bio-AgNPs	74.5 ± 3.9	37.2%	66.3 ± 3.7	36.4%	215.8 ± 10.8	41.0%
	Standalone Vancomycin	98.6 ± 4.8	16.9%	89.5 ± 4.1	14.1%	311.2 ± 12.7	14.8%
	Synergistic Combo	**29.4 ± 1.9**	**75.2%**	**31.8 ± 2.1**	**69.5%**	**72.6 ± 4.1**	**80.1%**

As outlined in Table 5, the synergistic combination against *P. aeruginosa* reduced total exopolysaccharide content from 142.5 ± 6.8 µg/mg down to 33.1 ± 2.3 µg/mg (a 76.8% reduction) and lowered matrix proteins from 88.4 ± 4.2 µg/mg down to 25.3 ± 1.8 µg/mg (a 71.4% reduction). Crucially, eDNA content dropped by 82.5%, decreasing from 486.2 ± 18.5 ng/mg to 85.1 ± 5.4 ng/mg. Similar degradation profiles occurred in MRSA biofilms, with matrix carbohydrates, proteins, and eDNA depleted by 75.2%, 69.5%, and 80.1%, respectively. Because eDNA maintains mechanical stability and mediates horizontal gene exchange within the matrix, its depletion reflects substantial loss of biofilm integrity.

3.5. Microscopic Architectural Breakdown via CLSM

Confocal laser scanning microscopy (CLSM) coupled with COMSTAT image analysis verified the architectural destruction of treated biofilms (Figure 3).

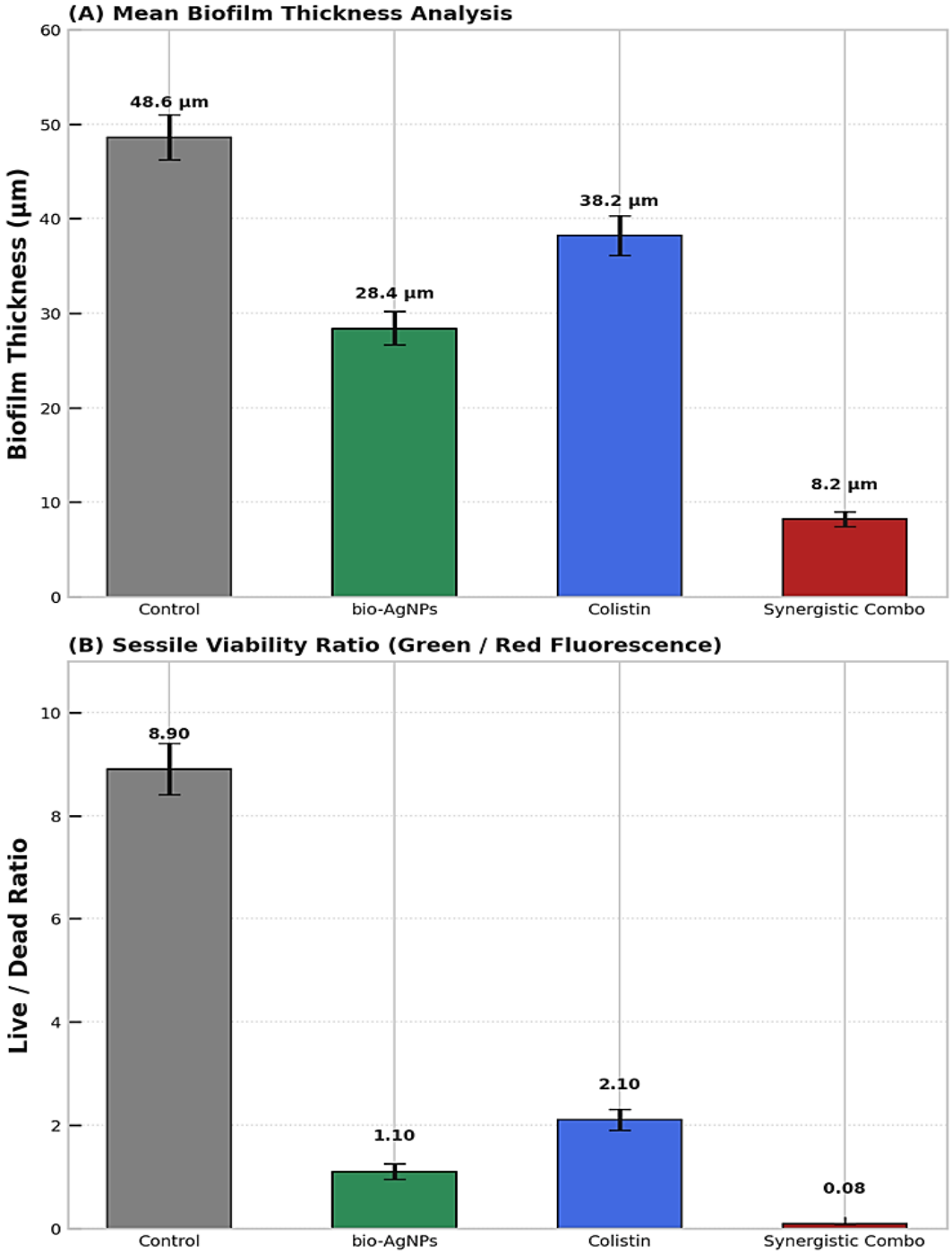


Figure 3: Confocal laser scanning microscopy (CLSM) analysis of *P. aeruginosa* biofilms following synergistic treatment. Three-dimensional reconstruction of untreated control biofilms with a thick layer of green, viable cells (A), comparison of the biofilm architecture with the synergistic combination-treated biofilms showing collapse of the architecture and strong red propidium iodide fluorescence (B), quantitative reduction in mean biofilm thickness (C), and green-to-red volumetric fluorescence ratio, which confirmed the loss of over 92% of cell viability (D).

The untreated *P. aeruginosa* biofilm was continuous and tightly packed with the majority of the fluorescence being green, from the SYTO 9 dye, and it had an average thickness of 48.6 ± 2.4 µm (Figure 3A). Contrastingly, biofilms treated with the synergistic combination (16.0 µg/mL bio-AgNPs + 4.0 µg/mL colistin) exhibited a disruption of their architecture with

scattered clusters, and with high red propidium iodide fluorescence (Figure 3B). COMSTAT analysis showed a drop from an average biofilm thickness of 83.1% (8.2 ± 0.8 μm) and a ratio of green-to-red fluorescence of 8.9 ± 0.5 to 0.08 ± 0.01, indicating more than 92% of the remaining attached bacteria were compromised.

3.6. Biocompatibility and Cytotoxicity Profiling

The synergistic combinations were found to be safe in vitro. The synergistic concentration of bio-AgNPs against *P. aeruginosa* (2.0 μg/mL) showed hemolysis of human red blood cell (1.82 ± 0.14%) which was under the safe clinical limit of 5.0%. The hemolysis was also minimal at 2.41 ± 0.19% when the bio-AgNPs were present at their synergistic concentration against MRSA (4.0 μg/mL). The hemolysis rates of the planktonic monotherapy MICs of standalone bio-AgNPs were 6.84% ± 0.42% and 12.35% ± 0.68% for 16.0 and 32.0 μg/mL, respectively. The synergistic combinations resulted in L929 fibroblasts remaining viable at 93.4 ± 2.1% after 24 h, whereas bio-AgNPs alone were found to be non-toxic for cells with concentration of 32.0 μg/mL, as the viability was 54.2 ± 3.4%. These tests show that the synergy effect of the 8-fold dose reduction provides an effective dose window, with low toxicity.

4. Discussion

The results of this study show that the use of microbially synthesized silver nanoparticles (bio-AgNPs) in combination with conventional antibiotics is one of the effective ways of overcoming the resistance that occurs at the level of biofilms in the presence of MDR P. aeruginosa and MRSA (Moradi et al., 2023). Biofilm-associated infections are challenging to treat clinically due to acquired genetic resistance mechanisms as well as physical diffusion barriers presented by the EPS matrix (Sahli et al., 2022). The average diameter of core was 18.4 nm and apparent hydrodynamic diameter of 32.8 nm for the bio-AgNPs produced by B. subtilis ATCC 6633 (Mikhailova, 2024). This small physical size allows for easy diffusion through water channels and interstitial voids of the EPS matrix with dimensions between 20 and 50 nm, which is far less than the surface steric entrapment encountered with larger chemically synthesized nanoparticles (Joshi et al., 2020).

The fractional inhibitory concentration index (FICI) value of 0.250 for both bacterial targets suggests that there is strong pharmacological synergy, below the normal value of 0.500 (Masadeh et al., 2024). This synergic effect is based on complementary effect mechanisms in the bacterial membrane (Hetta et al., 2023). The release of silver ions (Ag+) by bio-AgNPs is continuous that leads to the binding of these ions to avidly the outer-membrane proteins that have sulfhydryl (−SH), amino and carboxyl groups and disrupts the transmembrane electrical potential and structural integrity (Girma et al., 2024). For Gram-negative P. aeruginosa, this destabilization is coupled with the destabilization that occurs after the addition of colistin, which removes stabilizing divalent magnesium (Mg^{2+}) and calcium (Ca^{2+}) cations from molecules of lipopolysaccharide (LPS) (Kamer et al., 2024). This concerted action results in higher permeability of the outer membrane to allow Ag^{+} ions and antibiotics to enter the periplasmic space and the cytoplasm (Kamer et al., 2024). MRSA, however, weakens peptidoglycan cross-linking for vancomycin to reach its targets in the terminal D-Ala-D-Ala, which results in the ability of the antibiotic to work at lower concentrations (Gupta et al., 2018).

This combination's major therapeutic advantage is its ability to break down pre-formed, mature biofilms (Qayyum & Khan, 2016). The synergic formulations were more effective in the removal of over 86% of the biomass of the mature biofilm and viable sessile cell counts were reduced by more than 5.2 $\log_{10}$ CFU/mL compared to the antibiotic monotherapies alone (Qayyum & Khan, 2016). The biochemical profiling showed a considerable depletion in major matrix constituents such as carbohydrates (76.8 %), proteins (71.4 %) and eDNA (82.5%) (Qayyum et al., 2017). This matrix breakdown is facilitated by part of the generation of localized reactive oxygen species (ROS) such as hydroxyl radicals (OH•) and superoxide anions ($O_2^{\bullet -}$) via nanoparticles, which trigger oxidative degradation of the glycosidic bonds and the breaking of

the phosphodiester bonds of the EPS scaffold (Qayyum et al., 2017). The loss of eDNA is particularly significant, because eDNA gives the structure, helps maintain flow channels and protects bacteria from antimicrobial peptides with positive charge (Saffari Natanzi et al., 2025). The stability and safety profile of the biological origin of the nanoparticles has a significant role (Chaturvedi & Ranjan, 2025). Self-aggregation is avoided in high ionic strength salts in the presence of a steric stabilization from the endogenous protein corona obtained from the secretome of B. subtilis (Chaturvedi & Ranjan, 2025). Additionally, this organic coating also provides control over the release of ions, reducing the sudden surge of ions that can cause non-specific toxicity in chemically synthesized AgNPs (Casals et al., 2025). As a result, hemolytic activity was found to be < 1.9%, and viability of mammalian fibroblasts was > 93% at their effective concentrations (Casals et al., 2025). Combined with their ability to lower the dose of colistin and vancomycin by 8-fold, this combination will decrease the risk of severe nephrotoxicity and ototoxicity caused by these reserve antibiotics (AlQurashi et al., 2025). In general, the use of microbially synthesized nanoparticles alongside conventional antimicrobials seems to be a promising approach to achieve eradication of recalcitrant MDR biofilms while ensuring a safe biocompatibility profile.

5. Conclusion

The current study has shown the efficacy of the combination of the microbially synthesized silver nanoparticles (bio-AgNPs) produced by the strain of Bacillus subtilis ATCC 6633 with conventional antibiotics in the eradication of MRSA and multidrug-resistant (MDR) Pseudomonas aeruginosa mature biofilms. The green synthesis route resulted in uniformly sized, spherical nanocrystals of 18.4 ± 2.6 nm in average core size and surface charge of −29.6 ± 1.4 mV — with an endogenous protein corona on their surface. The checkerboard microdilution assays showed good synergy, reducing the minimum inhibitory concentration (MIC) of colistin and vancomycin by 8-fold and the fractional inhibitory concentration index (FICI) was 0.250 for both MDR pathogens.

On 48 h-old biofilms, the synergistic combinations were able to kill biofilm biomass up to 88.4 ± 1.7% and viable sessile cells more than 5.2 $\log_{10}$ CFU/mL. The biochemical analysis revealed that this architectural collapse was caused by significant reductions (by 76.8%, 71.4% and 82.5% respectively) in the amount of structural carbohydrates, matrix proteins and structural eDNA present in the extracellular polymeric substance (EPS) matrix. The confocal laser scanning microscopy results also showed a significant reduction in the size of the biofilm layer, with a significant level of disruption to the membrane being present throughout the remaining population. Importantly, the 8-fold reduction in active concentrations resulted in low hemolytic activity (<1.9%) and preserved mammalian fibroblast viability (>93%). These findings highlight the potential of biogenic nano-antibiotic combinations as translational platforms for treating persistent biofilm-associated infections, providing a foundation for future in vivo efficacy and safety evaluations.

References

1) AlQurashi, D. M., AlQurashi, T. F., Alam, R. I., Shaikh, S., & Tarkistani, M. A. M. (2025). Advanced nanoparticles in combating antibiotic resistance: current innovations and future directions. *Journal of Nanotheranostics*, *6*(2), 9.

2) Baptista, P. V., McCusker, M. P., Carvalho, A., Ferreira, D. A., Mohan, N. M., Martins, M., & Fernandes, A. R. (2018). Nano-strategies to fight multidrug resistant bacteria—"A Battle of the Titans". *Frontiers in microbiology*, *9*, 1441.

3) Bharathi, D., & Lee, J. (2025). Recent trends in bioinspired metal nanoparticles for targeting drug-resistant biofilms. *Pharmaceuticals*, *18*(7), 1006.

4) Casals, E., Gusta, M. F., Bastus, N., Rello, J., & Puntes, V. (2025). Silver nanoparticles and antibiotics: A promising synergistic approach to multidrug-resistant infections. *Microorganisms*, *13*(4), 952.

5) Chaturvedi, A., & Ranjan, R. (2025). Antimicrobial nanoparticles: a new horizon to combat multidrug-resistant bacteria. *Frontiers in Nanotechnology*, *7*, 1611126.

6) Ciofu, O., Moser, C., Jensen, P. Ø., & Høiby, N. (2022). Tolerance and resistance of microbial biofilms. *Nature Reviews Microbiology*, *20*(10), 621-635.

7) De Oliveira, D. M., Forde, B. M., Kidd, T. J., Harris, P. N., Schembri, M. A., Beatson, S. A., ... & Walker, M. J. (2020). Antimicrobial resistance in ESKAPE pathogens. *Clinical microbiology reviews*, *33*(3), 10-1128.

8) Flemming, H. C., Wingender, J., Szewzyk, U., Steinberg, P., Rice, S. A., & Kjelleberg, S. (2016). Biofilms: an emergent form of bacterial life. *Nature Reviews Microbiology*, *14*(9), 563-575.

9) Gallo, G., & Schillaci, D. (2021). Bacterial metal nanoparticles to develop new weapons against bacterial biofilms and infections. *Applied microbiology and biotechnology*, *105*(13), 5357-5366.

10) Girma, A., Alamnie, G., Bekele, T., Mebratie, G., Mekuye, B., Abera, B., ... & Jufar, D. (2024). Green-synthesised silver nanoparticles: antibacterial activity and alternative mechanisms of action to combat multidrug-resistant bacterial pathogens: a systematic literature review. *Green Chemistry Letters and Reviews*, *17*(1), 2412601.

11) Gupta, A., Landis, R. F., Li, C. H., Schnurr, M., Das, R., Lee, Y. W., ... & Rotello, V. M. (2018). Engineered polymer nanoparticles with unprecedented antimicrobial efficacy and therapeutic indices against multidrug-resistant bacteria and biofilms. *Journal of the American Chemical Society*, *140*(38), 12137.

12) Hall, C. W., & Mah, T. F. (2017). Molecular mechanisms of biofilm-based antibiotic resistance and tolerance in pathogenic bacteria. *FEMS microbiology reviews*, *41*(3), 276-301.

13) Hetta, H. F., Ramadan, Y. N., Al-Harbi, A. I., A. Ahmed, E., Battah, B., Abd Ellah, N. H., ... & Donadu, M. G. (2023). Nanotechnology as a promising approach to combat multidrug resistant bacteria: a comprehensive review and future perspectives. *Biomedicines*, *11*(2), 413.

14) Jamkhande, P. G., Ghule, N. W., Bamer, A. H., & Kalaskar, M. G. (2019). Metal nanoparticles synthesis: An overview on methods of preparation, advantages and disadvantages, and applications. *Journal of drug delivery science and technology*, *53*, 101174.

15) Joshi, A. S., Singh, P., & Mijakovic, I. (2020). Interactions of gold and silver nanoparticles with bacterial biofilms: Molecular interactions behind inhibition and resistance. *International journal of molecular sciences*, *21*(20), 7658.

16) Kamer, A. M. A., El Maghraby, G. M., Shafik, M. M., & Al-Madboly, L. A. (2024). Silver nanoparticle with potential antimicrobial and antibiofilm efficiency against multiple drug resistant, extensive drug resistant Pseudomonas aeruginosa clinical isolates. *BMC microbiology*, *24*(1), 277.

17) Koo, H., Allan, R. N., Howlin, R. P., Stoodley, P., & Hall-Stoodley, L. (2017). Targeting microbial biofilms: current and prospective therapeutic strategies. *Nature Reviews Microbiology*, *15*(12), 740-755.

18) Makabenta, J. M. V., Nabawy, A., Li, C. H., Schmidt-Malan, S., Patel, R., & Rotello, V. M. (2021). Nanomaterial-based therapeutics for antibiotic-resistant bacterial infections. *Nature Reviews Microbiology*, *19*(1), 23-36.

19) Masadeh, M. M., Al-Tal, Z., Khanfar, M. S., Alzoubi, K. H., Sabi, S. H., & Masadeh, M. M. (2024). Synergistic effect of silver nanoparticles with antibiotics for eradication of pathogenic biofilms. *Current Pharmaceutical Biotechnology*, *25*(14), 1884-1903.

20) Mikhailova, E. O. (2024). Green silver nanoparticles: an antibacterial mechanism. *Antibiotics*, *14*(1), 5.

21) Moradi, F., Ghaedi, A., Fooladfar, Z., & Bazrgar, A. (2023). Recent advance on nanoparticles or nanomaterials with anti-multidrug resistant bacteria and anti-bacterial biofilm properties: A systematic review. *Heliyon*, *9*(11).

22) Murray, C. J., Ikuta, K. S., Sharara, F., Swetschinski, L., Aguilar, G. R., Gray, A., ... & Tasak, N. (2022). Global burden of bacterial antimicrobial resistance in 2019: a systematic analysis. *The lancet*, *399*(10325), 629-655.

23) Pechnikova, N. A., Poimenidou, M., Patsidou, C., Zafeiriou-Chatziefraimidou, M., Iliadis, I., & Yaremenko, A. V. (2026). Engineered nanoparticles for combating drug-resistant bacteria and bacterial biofilms. *ACS Nano Medicine*, *1*(3), 492-546.

24) Pelgrift, R. Y., & Friedman, A. J. (2013). Nanotechnology as a therapeutic tool to combat microbial resistance. *Advanced drug delivery reviews*, *65*(13-14), 1803-1815.

25) Qayyum, S., & Khan, A. U. (2016). Nanoparticles vs. biofilms: a battle against another paradigm of antibiotic resistance. *MedChemComm*, *7*(8), 1479-1498.

26) Qayyum, S., Oves, M., & Khan, A. U. (2017). Obliteration of bacterial growth and biofilm through ROS generation by facilely synthesized green silver nanoparticles. *PloS one*, *12*(8), e0181363.

27) Saffari Natanzi, A., Poudineh, M., Karimi, E., Khaledi, A., & Haddad Kashani, H. (2025). Innovative approaches to combat antibiotic resistance: integrating CRISPR/Cas9 and nanoparticles against biofilm-driven infections. *BMC medicine*, *23*(1), 486.

28) Sahli, C., Moya, S. E., Lomas, J. S., Gravier-Pelletier, C., Briandet, R., & Hémadi, M. (2022). Recent advances in nanotechnology for eradicating bacterial biofilm. *Theranostics*, *12*(5), 2383.

29) Souza, G. M., de Oliveira Vieira, K. C., Naldi, L. V., Pereira, V. C., & Winkelstroter, L. K. (2021). Green synthesized nanoparticles as a promising strategy for controlling microbial biofilm. In *Nanotechnology for advances in medical microbiology* (pp. 1-28). Singapore: Springer Nature Singapore.

30) Yan, J., & Bassler, B. L. (2019). Surviving as a community: antibiotic tolerance and persistence in bacterial biofilms. *Cell host & microbe*, *26*(1), 15-21.